

# Modified Expanded Corrole–Ferrocene Conjugates: Syntheses, Structure and Properties

Rajeev Kumar,<sup>[a]</sup> Rajneesh Misra,<sup>[a]</sup> Viswanathan PrabhuRaja,<sup>[a]</sup> and Tavarekere K. Chandrashekar<sup>\*[a, b]</sup>

**Abstract:** Syntheses, characterization and properties of expanded corrole–ferrocene conjugates are reported. Ferrocenyl group are covalently linked to the corrole macrocycle through three different spacers groups. The synthetic strategy involved prior insertion of ferrocene with spacers to the dipyrromethane unit followed by a “3+2” acid-catalyzed oxidative coupling methodology. The optical and emission data of the expanded corrole–ferrocene conjugates depend on the nature and length of the spacer groups and the maximum effects are seen where ferrocene is directly linked to the *meso* carbon of macrocycle. The single crystal X-ray

structure of two expanded corrole–ferrocene conjugates; [22]pentaphyrin (1.1.0.1.0) with different *meso* substituents, clearly reveal shortening of the C–C bond length linking the *meso* carbon and the aryl substituent containing the ferrocene moiety relative to *meso* aryl substituents without ferrocene. The results suggest that an electronic interaction between the two  $\pi$  systems. Electrochemical data reveal harder oxidation for the ferrocene unit in the conjugates relative to free ferro-

cene; this suggests the electron donating nature of the ferrocene. The first corrole ring oxidation shows easier oxidation relative to **1** and the magnitude of shifts in potential is inversely proportional to the length of spacer. The molecular first hyperpolarizabilities ( $\beta$ ) measured at 1064 nm by HRS method vary in the range  $20\text{--}32 \times 10^{-30}$  esu and imply that the  $\beta$  values can be increased by enhancing the number of mobile electrons in the conjugation. The conjugates form 1:1 metal complex with the Rh<sup>I</sup> where rhodium is coordinated to one amino and one imino nitrogen of the dipyrromethane unit.

**Keywords:** corroles • ferrocenes • nonlinear optics • porphyrinoids

## Introduction

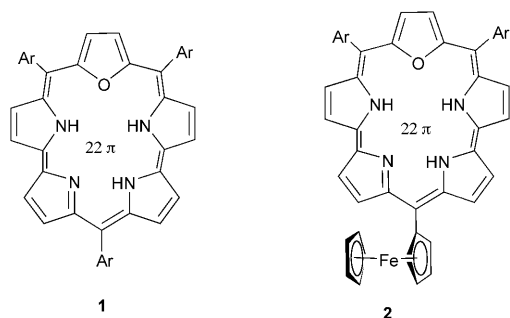
Porphyrins and corroles occur in many natural systems performing diverse functions.<sup>[1]</sup> Even though both have  $18\pi$  electrons in conjugation, they are structurally different. In porphyrins the four pyrrole rings are linked through four *meso*-carbon bridges, whereas in the corrole the four pyrrole rings are linked with only three *meso* carbons with one direct pyrrole–pyrrole link. This structural differentiation leads to difference in electronic structure and hence variations in the spectral and electrochemical properties. Porphyrins can be expanded by increasing the number of pyr-

role rings in conjugation and a range of expanded porphyrins<sup>[2,3]</sup> such as sapphyrins, rubyrins, hexaphyrin, heptaphyrins and octaphyrins have been reported in the literature. In a similar fashion the corrole macrocycle can also be expanded by introducing a larger number of heterocyclic rings and increasing the number of direct pyrrole–pyrrole links leading to the formation of expanded corroles. Studies on expanded corroles are limited in the literature<sup>[4a]</sup> and recently we have reported the syntheses and characterization of expanded corroles<sup>[4b,c]</sup> **1**; its properties resemble that of a corrole rather than a porphyrin.

The linkage of a redox active group/luminescent group to a molecular  $\pi$  system results in the formation of discrete molecular conjugates.<sup>[5]</sup> Such conjugates exhibit electronic interactions between the redox active group/luminescent group and the molecular  $\pi$  system.<sup>[6]</sup> Recently we have reported the synthesis of such a conjugate **2** in which the redox active ferrocene group is covalently linked to the expanded corrole system at the *meso*-carbon position.<sup>[7a]</sup> In continuation of our project on molecular conjugates for application in molecular devices,<sup>[8]</sup> we report herein the syn-

[a] R. Kumar, R. Misra, V. PrabhuRaja, Prof. Dr. T. K. Chandrashekar  
Department of Chemistry, Indian Institute of Technology  
Kanpur 208 016 (India)  
E-mail: tkc@iitk.ac.in

[b] Prof. Dr. T. K. Chandrashekar  
Regional Research Laboratory, Trivandrum  
Kerala 695019 (India)  
Fax: (+91) 471-249-1712

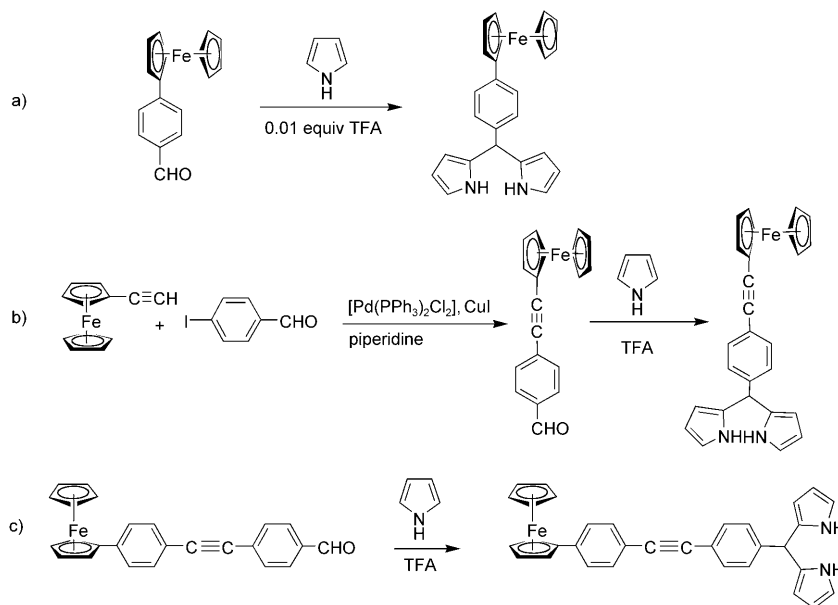


theses, characterization and properties of expanded corrole–ferrocene conjugates in which an expanded corrole is linked to a ferrocene group via different spacer groups. These expanded corrole–ferrocene conjugates are not only important from the synthetic point of view but are also expected to show different electronic properties. Specifically in this paper we wish to report the syntheses and characterization of expanded corrole–ferrocene conjugates linked through three different spacer groups: a simple phenyl spacer, a phenyl spacer linked to an acetylene moiety and two phenyl spacers sandwiched by an acetylene moiety to understand the effect of spacer groups on the electronic interaction of the ferrocene  $\pi$  system and the expanded corrole  $\pi$  system. Spectroscopic and electrochemical studies reveal a moderate interaction between the ferrocene group and the corrole  $\pi$  system. The molecular first hyperpolarizabilities ( $\beta$ ) measured for these conjugates are moderate ( $20\text{--}32 \times 10^{-30}$  esu). These data are discussed in terms of orientation of the ferrocene and the corrole moiety with respect to the spacer group.

## Results and Discussion

**Syntheses:** The expanded corrole–ferrocene conjugates were synthesized by a two-step procedure. Our strategy was to incorporate the ferrocene moiety with the appropriate spacer into one of the precursors that is, the dipyrromethane unit. This was achieved by reaction of ferrocene containing aldehyde with excess pyrrole in presence of 0.1 equiv of trifluoroacetic acid (TFA) as catalyst to give dipyrromethane ferrocene moieties **3–5** as depicted in Scheme 1. The dipyrromethanes are found to be stable at room temperature without any noticeable decomposition. Furthermore dipyr-

romethane **3** was characterized by single crystal X-ray crystallographic analysis and the structure is shown in Figure 1. It is seen in Figure 1 that the *meso* phenyl ring is almost perpendicular to dipyrromethane unit (dihedral angle;  $73.9^\circ$ ) and the ferrocene ring which is attached to C13 carbon atom of phenyl ring is almost planar (dihedral angle;  $14.2^\circ$ ). There are no significant changes in the bond lengths of the ferrocene groups upon linking to dipyrromethane unit. The C–C bonds C16–C13, which connect the ferrocene group to the phenyl ring is  $1.474 \text{ \AA}$  long and the length of the C–C



Scheme 1. Syntheses of dipyrromethanes **3–5**.

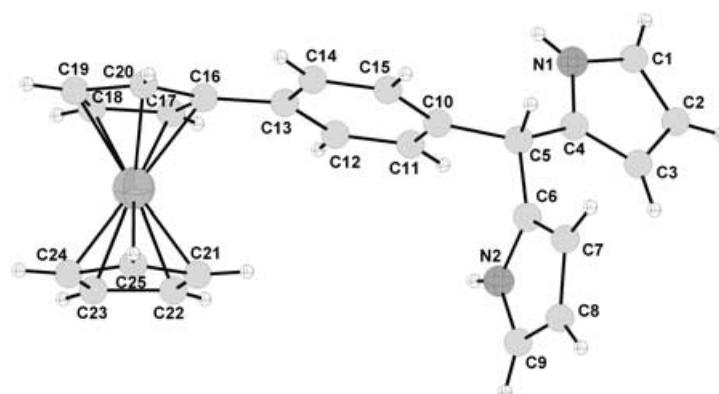


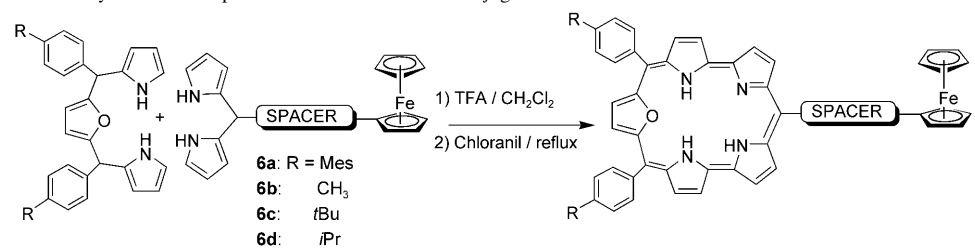
Figure 1. Single crystal X-ray structure of **3**.

bond C10–C5, is  $1.528 \text{ \AA}$ . The dihedral angle between the phenyl ring and the Cp ring of ferrocene is  $14.22^\circ$ .

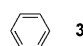
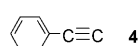
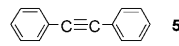
In the second step, the standard acid catalyzed “3+2” oxidative coupling methodology using the required oxa-tripyrane and dipyrromethane was used to construct the required expanded corrole–ferrocene conjugates, where two direct

pyrrole–pyrrole bonds were generated in a single step.<sup>[4b,c]</sup> The oxa-triopyrranes **6a–d** were synthesized by our previous method.<sup>[9]</sup> Thus acid catalyzed coupling reactions between dipyrromethanes **3–5** with various *para*-substituted 5,10-diphenyl-16-oxa-triopyrranes **6a–d** gave ferrocenyl expanded corroles **7a–9c** as the major products in  $\approx 25\%$  yield (Table 1). Trace amounts of the monooxa porphyrin<sup>[10]</sup> and

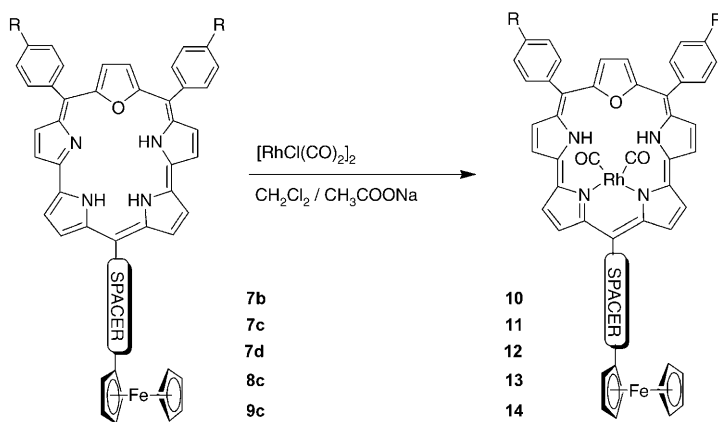
Table 1. Syntheses of expanded corrole–ferrocene conjugates.



6a: R = Mes  
6b: CH<sub>3</sub>  
6c: *t*Bu  
6d: *i*Pr

Spacer in dipyrromethane	Triopyrrane	Conjugates
 <b>3</b>	<b>6a</b>	<b>7a</b>
	<b>6b</b>	<b>7b</b>
	<b>6c</b>	<b>7c</b>
	<b>6d</b>	<b>7d</b>
 <b>4</b>	<b>6a</b>	<b>8a</b>
	<b>6b</b>	<b>8b</b>
	<b>6c</b>	<b>8c</b>
 <b>5</b>	<b>6a</b>	<b>9a</b>
	<b>6b</b>	<b>9b</b>
	<b>6c</b>	<b>9c</b>

rubyrin<sup>[11]</sup> were also formed as side products. The desired product was separated by silica gel column chromatography. These conjugates were found to be stable as freebase in the solid and solution phases. The rhodium complexes **10–14** were synthesized by the reaction of freebase with di- $\mu$ -chlorobis[dicarbonylrhodium(i)] in the presence of sodium acetate. The purification was performed with silica gel column chromatography. The complexes **10–14** were also to be found stable at room temperature (Scheme 2).



Scheme 2. Syntheses of rhodium complexes of expanded corrole–ferrocene conjugates.

**Spectral characterization:** All the compounds reported here were characterized by FAB-MS, UV/Vis, <sup>1</sup>H and 2D NMR spectroscopy. For example the FAB mass spectrum of **7d** displays a molecular ion peak *m/z* (%) at 861 (100) confirming the proposed composition. The corresponding rhodium complex **12** exhibits peak at *m/z* 1018 (65). Furthermore the presence of the carbonyl groups in the rhodium complex were confirmed by infrared spectroscopy, which displayed peaks at 2072 and 2007 cm<sup>-1</sup> for **12**. These frequencies compare well with rhodium carbonyl complexes reported in the literature.<sup>[12]</sup> These metal complexes are highly sensitive to acid and common mineral acids were found to demetallate the complexes giving the corresponding freebase derivatives.

**<sup>1</sup>H NMR spectroscopy:** A detailed analysis of <sup>1</sup>H and 2D NMR spectra of **7a–9c** confirms the proposed solution structures. The <sup>1</sup>H NMR spectra of **7a–9c** were well resolved in freebase form and all the assignments were based on the correlations observed in the <sup>1</sup>H/<sup>1</sup>H COSY spectrum. For example the <sup>1</sup>H/<sup>1</sup>H COSY spectrum

in the aromatic region observed for **7d** is shown in Figure 2 and the correlations observed are marked. Briefly, the pyrrolic protons (b, b'; c, c'; d, d'; e, e') resonate as four well-resolved doublets in the region 8–10 ppm with coupling constants 4–4.4 Hz. The outer pyrrolic protons (b, b'; e, e') are more shielded as compared to the inner pyrrolic protons (c, c'; d, d') because of the upfield ring current contribution of the *meso*-aryl ring. The  $\beta$ -CH protons of the furan ring (a, a') appear as a sharp singlet at 8.67 ppm. There are two sets of aromatic protons in the phenyl ring containing the isopropyl groups, the protons present next to carbon atom connected to *meso* position (n) resonate as doublet at  $\delta$  8.03 and the other two protons (m) resonate as doublet at  $\delta$  7.57. Similarly in the 4-ferrocenylphenyl ring, protons present next to carbon atom connected to *meso* position (f, f') resonate as doublet at  $\delta$  7.87 and the other two protons (g, g') resonate as doublet at  $\delta$  8.24. There are three sets of protons in the ferrocenyl group, the protons present next to carbon, which is connected to phenyl ring (h), resonate at  $\delta$  4.86 and other two protons (i) resonate at  $\delta$  4.42 and the other cyclopentadienyl ring protons resonate as singlet at  $\delta$  4.19. The equivalence of these pyrrolic protons (b, b'; c, c'; d, d'; e, e') in the <sup>1</sup>H NMR spectrum suggest that the molecule adopts a symmetric conformation in solution with respect to the mirror plane passing through the methine bridge connecting 4-ferrocenylphenyl and the furan oxygen atom. This is possi-

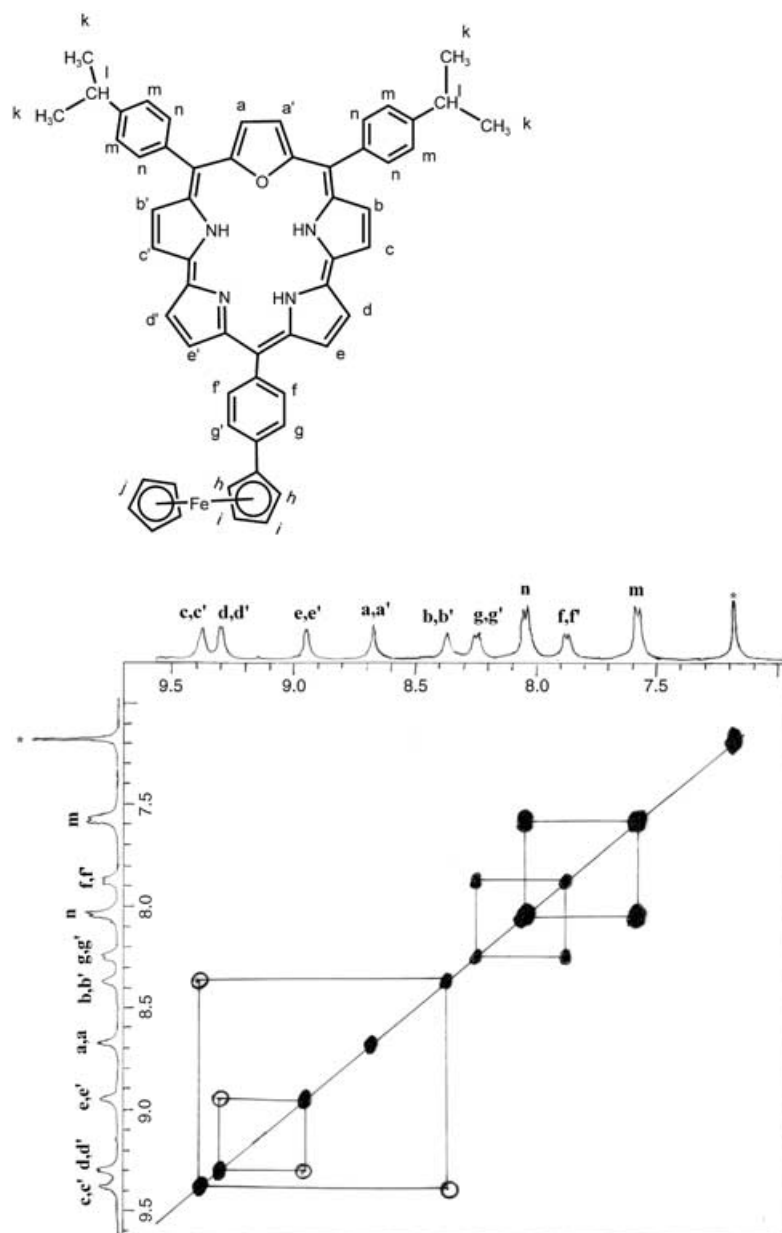


Figure 2.  $^1\text{H}/^1\text{H}$  COSY spectrum of **7d** in  $\text{CDCl}_3$  at room temperature. The observed correlations and the assignment are marked.

ble only if there is a rapid tautomerism between the inner NH protons indicating the three NH protons exchange sites between four bipyrrrole nitrogen centers. Upon lowering the temperature to 240 K, no NH signals were observed, which indicates tautomerism even at 240 K. Introduction of  $\text{Rh}^{\text{I}}$  to expanded corrole–ferrocene conjugates gives the corresponding rhodium complexes where rhodium is bound in an  $\eta^2$  fashion to two of the four core nitrogens with other two coordination sites on rhodium is taken by the ancillary carbonyl ligands. A typical  $^1\text{H}$  NMR spectrum observed for **13** is shown in Figure 3. The metallation with rhodium arrest the NH tautomerism and the NH protons, which are not coordinating to rhodium metal, now appear as a singlet at  $\delta$

–1.77 (Figure 3, inset), supporting the presence of NH tautomerism in the freebase. The metallation leads to interesting changes in the NMR spectrum. Specifically, i) the pyrrolic protons (d, d'; e, e') which are in the dipyrromethane unit, experience an upfield shift (0.11 ppm), ii) the pyrrolic protons (b, b'; c, c'), which are in the tripyrrane unit, experience a downfield shift (0.13 and 0.17 ppm), iii) the pyrrolic protons (b, b'; c, c') appear as quartets ( $^4J_{\text{H,H}} = 2.2$  Hz), while the pyrrolic protons (d, d'; e, e') appear as doublets ( $J_{\text{AB}} = 4.2$  Hz), iv) the furan protons also experience a downfield shift and appear as a singlet at 9.19 ppm. These observations further confirms our earlier findings that the  $\text{Rh}^{\text{I}}$  binds to the dipyrromethane unit with one amino and one imino nitrogen.<sup>[12a]</sup>

#### Electronic absorption spectra:

Typical electronic absorption spectra observed for expanded corrole–ferrocene conjugates; **7a**, **8a** and **9a** are shown in Figure 4. A strong Soret-type band in the region 440–455 nm and four Q-bands in the region 500–750 nm confirm the porphyrinic nature.<sup>[2]</sup> The UV/Vis data are tabulated in Table 2. The following observations are made from the data in the table: i) the introduction of spacers between ferrocene and the macrocycle results in a

bathochromic shift of both Soret and Q-bands relative to **1**. The magnitude of the Q-band shifts is higher (500–3900  $\text{cm}^{-1}$ ) than those for the Soret band (150–400  $\text{cm}^{-1}$ ) and is similar to that observed for the porphyrins.<sup>[2]</sup> There is a linear correlation between decrease in energy of Soret band and increment in number of spacers which is shown in Figure 5. ii) The  $\epsilon$  values of the expanded corrole–ferrocene conjugates are more than 30–50 % lower than those of **1** and more than **2** suggesting the presence of electronic interaction between the ferrocene and macrocyclic  $\pi$  system. iii) Protonation leads to a red shift of the Soret band and a decrease in the number of the Q-bands which is typical of *meso*-aryl porphyrins.<sup>[13]</sup> iv) Metallation of free base with

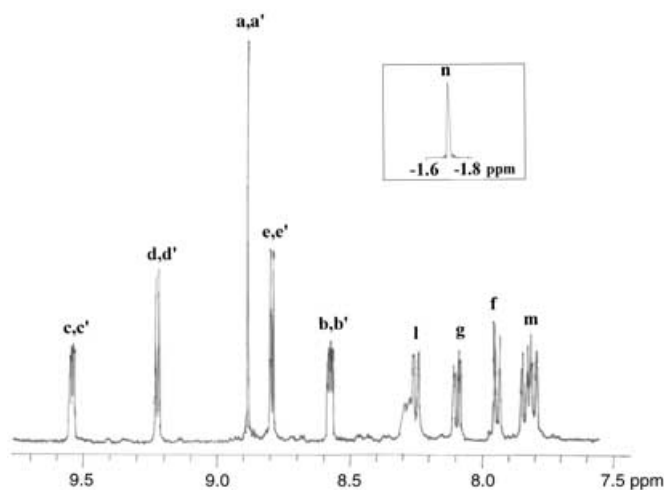
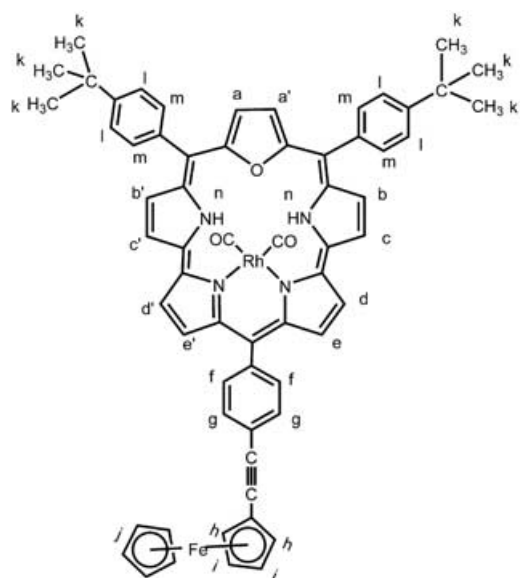


Figure 3.  $^1\text{H}$  NMR spectrum of **13** at room temperature in  $\text{CDCl}_3$  (inset shows pyrrole NH signal).

$\text{Rh}^{\text{I}}$  metal ion leads to a red shift and splitting of the Soret band. The splitting of the Soret band upon metallation suggests a lowering of the symmetry of the complexes as a result of a perturbation of the energy levels. v) The  $\epsilon$  values of the metallated derivative are about 50% smaller than those of corresponding free base derivatives suggesting a decreased  $\pi$ -electron conjugation upon metal insertion consistent with the lowering of the symmetry.

The emission spectra for compounds **7a–10** were recorded in  $\text{CH}_2\text{Cl}_2$ . Inset Figure 4 shows the emission spectra for compounds **7a**, **8a** and **9a**. The emission parameters are tabulated in Table 3. The quantum yields were calculated using tetraphenyl porphyrin as the reference compound ( $\phi = 0.11$ ) and the lifetime data was fitted satisfactorily to a biexponential curve with good  $\chi^2$  values (1.01–1.10), in most

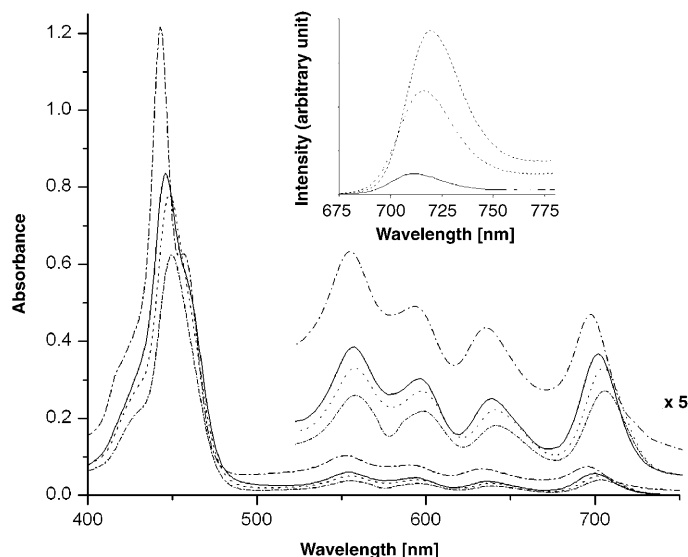


Figure 4. Electronic absorption and emission spectra of **7a** (—) ( $2.42 \times 10^{-6} \text{ M}$ ), **8a** (.....) ( $1.94 \times 10^{-6} \text{ M}$ ), **9a** (-----) ( $2.45 \times 10^{-6} \text{ M}$ ) and **1** (-·-·-) in  $\text{CH}_2\text{Cl}_2$  (inset shows emission spectra of **7a** (—), **8a** (.....) and **9a** (-----) in  $\text{CH}_2\text{Cl}_2$ ).

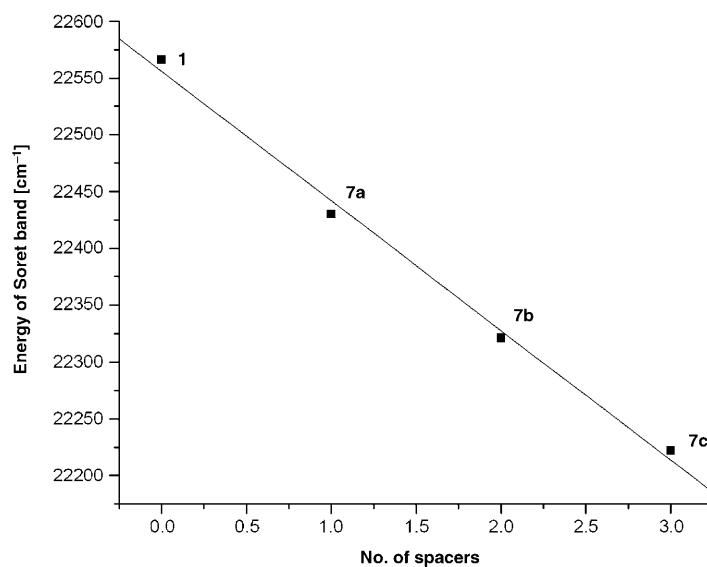


Figure 5. Plot of number of spacers versus energy of the Soret band.

cases. Since it is difficult to compare the two components of the life times, we determined an average emission lifetime,  $\langle \tau \rangle$ , for conjugates emission by using an expression described by James and co-workers.<sup>[14a]</sup> The radiative ( $k_r$ ) and non-radiative ( $k_{nr}$ ) decay were obtained by following expression.

$$k_r = \frac{\phi_f}{\tau} \quad (1)$$

Table 2. UV/Vis absorption data for expanded corrole–ferrocene conjugates in Soret and Q-bands region in dichloromethane ( $\approx 10^{-6}$  M).

Compound	$\lambda_{\text{max}}$ Soret [nm] [ $\epsilon \times 10^{-4}$ ( $\text{M}^{-1} \text{cm}^{-1}$ )]	$\lambda_{\text{max}}$ Q-bands [nm] [ $\epsilon \times 10^{-4}$ ( $\text{M}^{-1} \text{cm}^{-1}$ )]			
<b>1</b>	443 [33.1]	456 [16.2]	552 [2.1]	591 [1.4]	633 [1.54]
<b>7a</b>	447 [17.34]	554 [1.29]	594 [1.05]	637 [0.90]	700 [1.21]
<b>7b</b>	446 [18.95]	555 [1.41]	594 [1.08]	637 [0.88]	700 [1.34]
<b>7c</b>	446 [18.27]	554 [1.50]	594 [1.06]	637 [0.93]	700 [1.39]
<b>7d</b>	446 [18.25]	554 [1.49]	594 [1.08]	637 [0.90]	700 [1.31]
<b>8a</b>	450 [22.39]	557 [1.98]	597 [1.63]	639 [1.36]	703 [1.96]
<b>8b</b>	448 [21.68]	555 [1.51]	595 [1.20]	640 [0.92]	703 [1.47]
<b>8c</b>	448 [19.58]	556 [1.61]	595 [1.32]	639 [1.06]	703 [1.51]
<b>9a</b>	451 [23.21]	557 [1.63]	596 [1.31]	640 [1.06]	704 [1.55]
<b>9b</b>	450 [24.82]	556 [1.72]	594 [1.43]	640 [1.04]	704 [1.73]
<b>9c</b>	450 [24.62]	556 [1.31]	594 [1.11]	640 [0.94]	704 [1.62]
<b>10</b>	459 [14.65]	479 [1.21]	574 [1.58]	616 [1.32]	637 [1.52]
<b>11</b>	459 [14.66]	479 [0.93]	573 [1.77]	616 [1.52]	637 [1.40]
<b>12</b>	459 [12.98]	479 [0.78]	572 [1.48]	616 [1.25]	638 [1.14]
<b>13</b>	460 [18.68]	479 [1.54]	575 [1.13]	617 [0.87]	639 [1.21]
<b>14</b>	461 [19.95]	480 [1.63]	576 [1.35]	619 [0.95]	640 [1.38]

Table 3. Photophysical data of expanded corrole–ferrocene conjugates in  $\text{CH}_2\text{Cl}_2$  at 300 K.

Compound	$\lambda_{\text{abs}}$ [nm]	$\lambda_{\text{em}}$ [nm]	Stokes shift [ $\text{cm}^{-1}$ ]	$\phi_f$ ( $10^{-4}$ )	$\tau$ [ns]	$k_f \times 10^{-6}$ [ $\text{s}^{-1}$ ]	$k_{\text{nr}} \times 10^{-8}$ [ $\text{s}^{-1}$ ]
<b>7a</b>	447	713	8346	5.78	4.78	0.12	2.09
<b>7b</b>	446	714	8415	8.52	4.40	0.19	2.27
<b>7c</b>	446	714	8415	10.47	4.62	0.23	2.16
<b>7d</b>	446	714	8415	8.47	4.53	0.18	2.20
<b>8a</b>	450	716	8255	21.1	1.97	1.07	5.06
<b>8b</b>	448	719	8413	19.5	2.95	0.66	3.33
<b>8c</b>	448	719	8413	20.3	2.42	0.83	4.12
<b>9a</b>	451	717	8225	79.7	1.66	4.80	5.97
<b>9b</b>	450	719	8314	84.17	2.16	3.89	4.59
<b>9c</b>	450	720	8333	84.6	1.93	4.38	5.13
<b>12</b>	459	715	7800	4.56	3.79	0.11	2.63
<b>1</b>	443	706	8409	240	5.27	4.55	1.85

$$k_{\text{nr}} = \frac{(1 - \phi_f)}{\tau} \quad (2)$$

Inspection of Table 3 reveals the following; i) The quantum yield for these expanded corrole–ferrocene conjugates are 3–45-fold lower than **1** and increase in quantum yield is observed upon increase in length of spacers between ferrocene and the macrocycle. This observation clearly suggests that the substitution of ferrocenyl group quenches the fluo-

rescence of the expanded corroles and the magnitude of quenching depends upon the nature of the spacers, ii) regular emission band shift to lower energies upon increasing the spacer length, iii) the singlet lifetimes for **7a–9c** are lower relative to that of **1** and it decreases as the length of the spacer increases. In the present study, it has been observed that the  $k_{\text{nr}}$  values are about 1.5–3 times larger for the conjugates than **1**. The larger quantum yield for **9a–c** is consistent with the larger radiative  $k_f$  decay values at the expense of nonradiative  $k_{\text{nr}}$  decay values.<sup>[14b,c]</sup> A small decrease observed in the life time for **7a–9c** relative to **1** suggests that the rates of intersystem crossing and internal conversion are predominant in expanded corrole–ferrocene conjugates, relative to **1**.<sup>[4b]</sup>

**Crystallographic characterization:** The proposed structures of the expanded corrole–ferrocene conjugates were further confirmed by solving single crystal X-ray structure for **7a** and **7d** and are shown in Figures 7 and 8, respectively. In **7a**, one molecule of methanol is trapped inside the cavity. The important crystallographic parameters are listed in Table 4. The structure indicates small deviations from planarity (Figures 7b, 8b). The deviation of the heterocyclic rings in **7a** with respect to the mean expanded corrole plane (defined by three *meso* carbons C1, C6 and C15 which form the plane) are: for the furan, 5.07°; for the pyrrole N1 ring, 4.87°; for the pyrrole N2 ring, 10.01°; for the pyrrole N3 ring, 3.18°; for the pyrrole N4 ring, 2.49°; these deviations are similar to that observed for **1** and **2**, suggesting that there is not much structural deviation upon introduction of spacer. The dihedral angle between the expanded corrole plane and the phenyl ring containing the ferrocene group is

56° while the corresponding dihedral angle for the other phenyl rings are 89.3° and 85.2° respectively. This decrease in dihedral angle for the phenyl ring containing ferrocene group clearly suggests the presence of a moderate  $\pi$  interaction between the  $\pi$  system of cyclopentadienyl ring and corrole ring. This is further reflected in the C–C bond distances observed (Table 5). For example the C–C bond (C15–C42) connecting the 4-ferrocenylphenyl ring to the *meso*-carbon atom is 1.484 Å while corresponding bond

length (C5–C10) in the dipyrromethane **3** is 1.528 Å. Furthermore the C–C bond distance of the remaining two *meso* phenyl substituents (C1–C24; C6–C33) are 1.507 Å. Thus, the significant reduction in the bond distance of C15–C42 for **7a** is a reflection of presence of electronic coupling between the  $\pi$  systems. This C–C bond length 1.484 Å falls in the range of the distance observed for other ferrocene–porphyrin<sup>[7e]</sup> and *meso*-ferrocenyl–smaragdyrin conjugate<sup>[7a]</sup> sys-

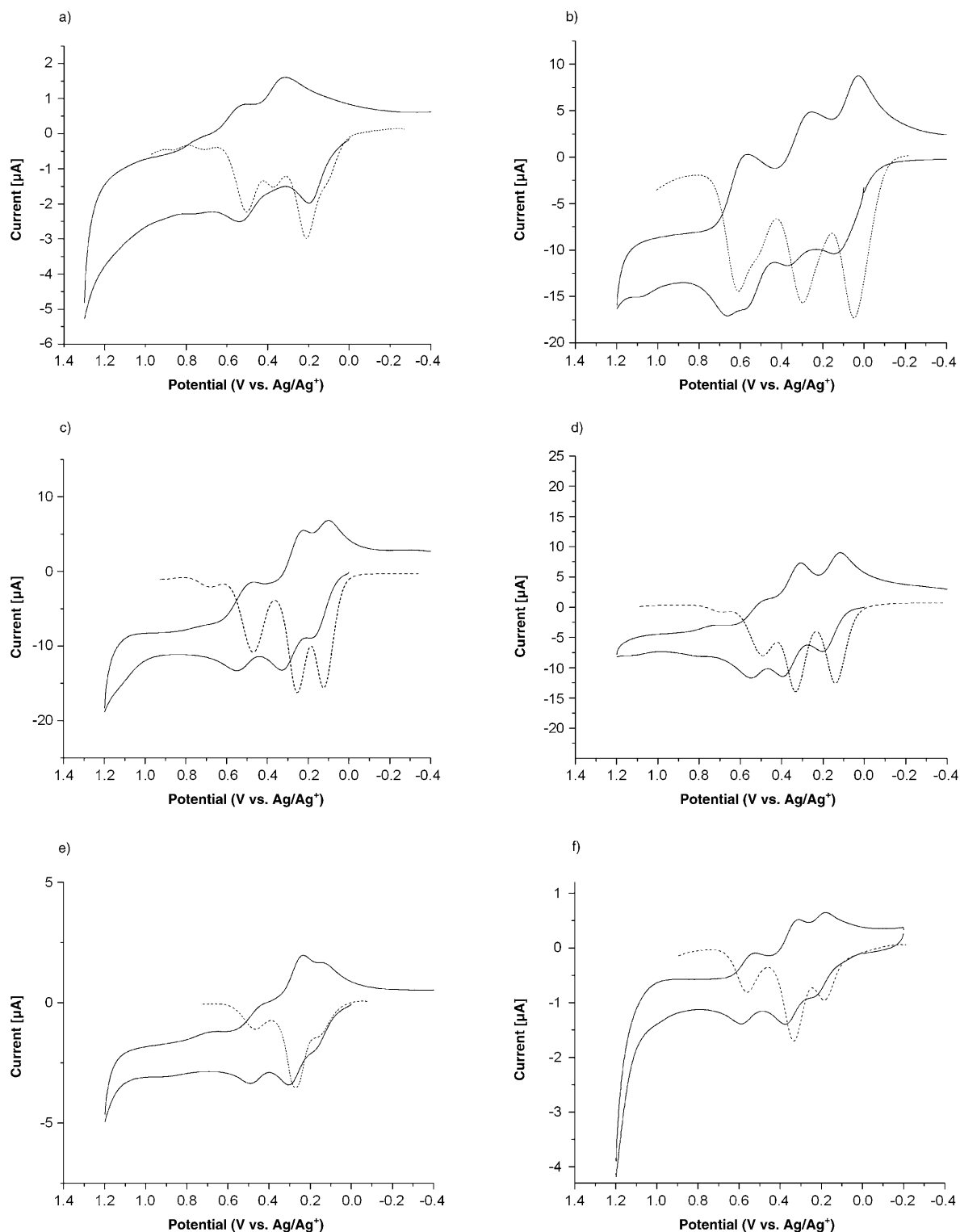


Figure 6. Cyclic voltammograms (—) and differential pulse voltammograms (-----) of a) **1**, b) **2**, c) **7a**, and d) **8a**, e) **9b** and f) **13** in  $\text{CH}_2\text{Cl}_2$  containing 0.1 M TBAPF<sub>6</sub>, recorded at 100  $\text{mV s}^{-1}$  scan speed.

tems [1.47–1.49 Å], where strong  $\pi$ -electronic communications are observed. A comparison of the important bond distances and dihedral angles of **3**, **7a** and **7d** is listed in Table 5. The aromatic nature of the 22  $\pi$  expanded corrole

is confirmed by the  $\text{C}_\beta$ – $\text{C}_\beta$  distances of heterocyclic rings. For example  $\text{C}_\beta$ – $\text{C}_\beta$  distance in furan ring is 1.353 Å, whereas  $\text{C}_\alpha$ – $\text{C}_\beta$  distance is 1.406 Å. This agrees well with data for expanded porphyrins reported in the literature.<sup>[2]</sup>

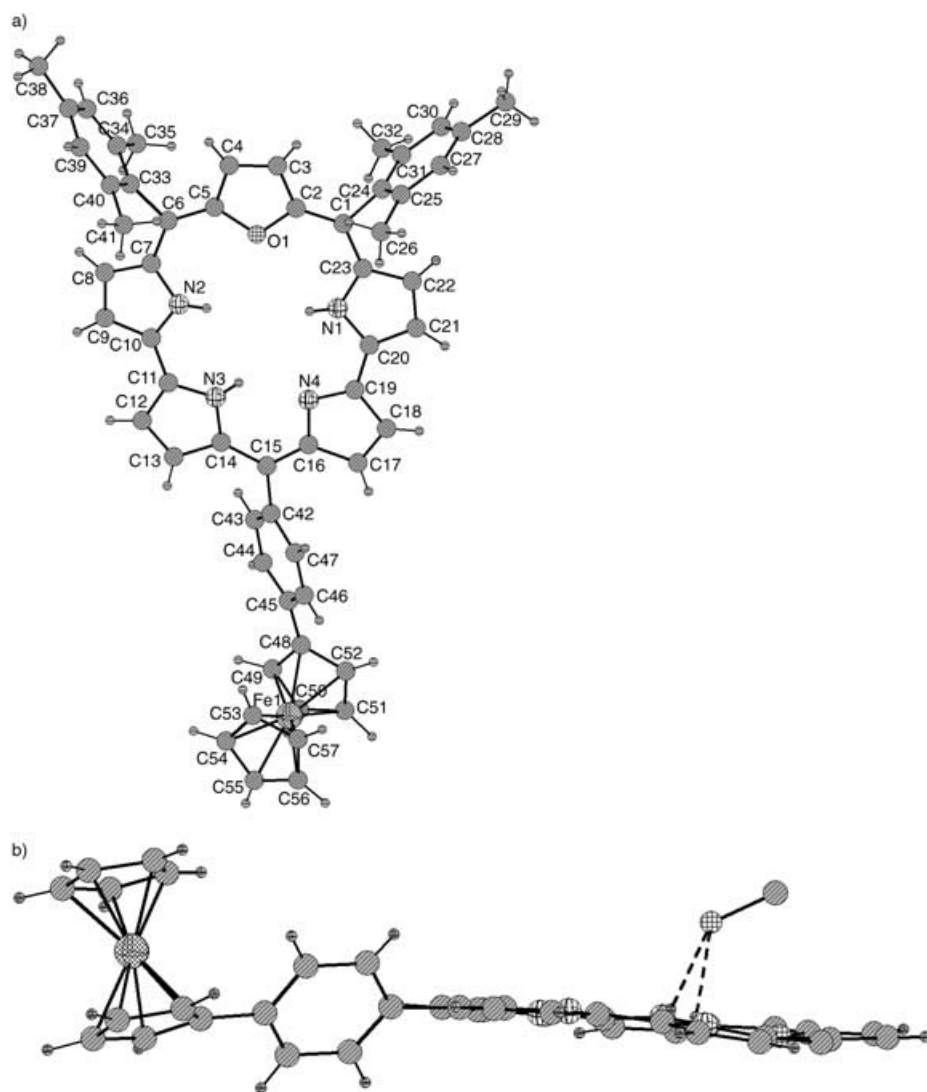


Figure 7. Single crystal X-ray structure of **7a** with one trapped methanol molecule a) top view; b) side view (*meso*-phenyl rings are omitted for clarity).

Another important observation on the crystal structure of **7a** is that one methanol solvent molecule is trapped inside the cavity of the macrocycle. The solvent methanol is held by two hydrogen-bonding interactions between the methanol oxygen and the hydrogen atoms attached to the pyrrole N1 and N2 rings (O2...H101, 2.617 Å, 138.1°; O2...H201, 2.317 Å, 136.3°).

**Electrochemical studies:** The redox behavior of various expanded corrole–ferrocene conjugates was monitored by cyclic voltammetric studies. Electrochemical data of expanded corrole–ferrocene conjugates, rhodium complexes along with free ferrocene, dipyrromethanes and the conjugates, are listed in Table 6. Some typical cyclic voltammograms overlaid with differential pulse voltammograms of expanded corroles in the positive potential region are shown in Figure 6. In general one would expect to see three couples; one for ferrocene and two for ring oxidations of expanded

corroles. From the table, the following important observations are apparent; i) the potential for the ferrocene couple is more positive in conjugates relative to free ferrocene, which suggests a harder oxidation of ferrocene in the conjugates; ii) the magnitude of the positive shift for the ferrocene couple depends on the nature of the spacers; the maximum shifts (117–127 mV) are observed for the spacer having  $-C\equiv C-Ph$  group; iii) the positive shift of the ferrocene couple clearly suggests that the ferrocene group is acting as an electron donor, pumping electron density to the corrole  $\pi$  system; iv) the expanded corrole ring shows two quasi-reversible oxidations and the first ring oxidation is easier than **1**, which indicates the electron acceptor nature of the expanded corrole  $\pi$  system. The maximum effect is seen (102 mV) for **2** since the ferrocene is directly attached to the corrole  $\pi$  skeleton. The second oxidation potential depends on the nature of the substituents. For mesityl substituents, the shifts are positive (12–27 mV) and for tolyl and *tert*-Bu substituents shifts are negative (12–36 mV); v) metallation of the corrole ring results in positive shift for the oxidation

in contrast to freebase. This is probably due to lowering of the symmetry of the macrocycle upon metallation. Thus taken together the electrochemical data clearly supports the electronic interaction between the ferrocene group and the expanded corrole ring.

**Nonlinear optical studies:** The electron donating behavior of the ferrocene group in expanded corrole conjugates prompted us to perform preliminary non linear optical studies for the suitability as second order non linear optical materials. We have measured the molecular first hyperpolarizabilities ( $\beta$ ) by hyper-Rayleigh scattering (HRS) method for compounds **7a–9c** and the  $\beta$  values are listed in Table 7. For the sake of comparison,  $\beta$  values are also measured for compound **1** and **2** by HRS method at 1064 nm. A typical linear dependence of HRS intensity on chromophore number density for **9b** is shown in Figure 9. From the slope of plot, we extracted hyperpolarizability values after comparison with



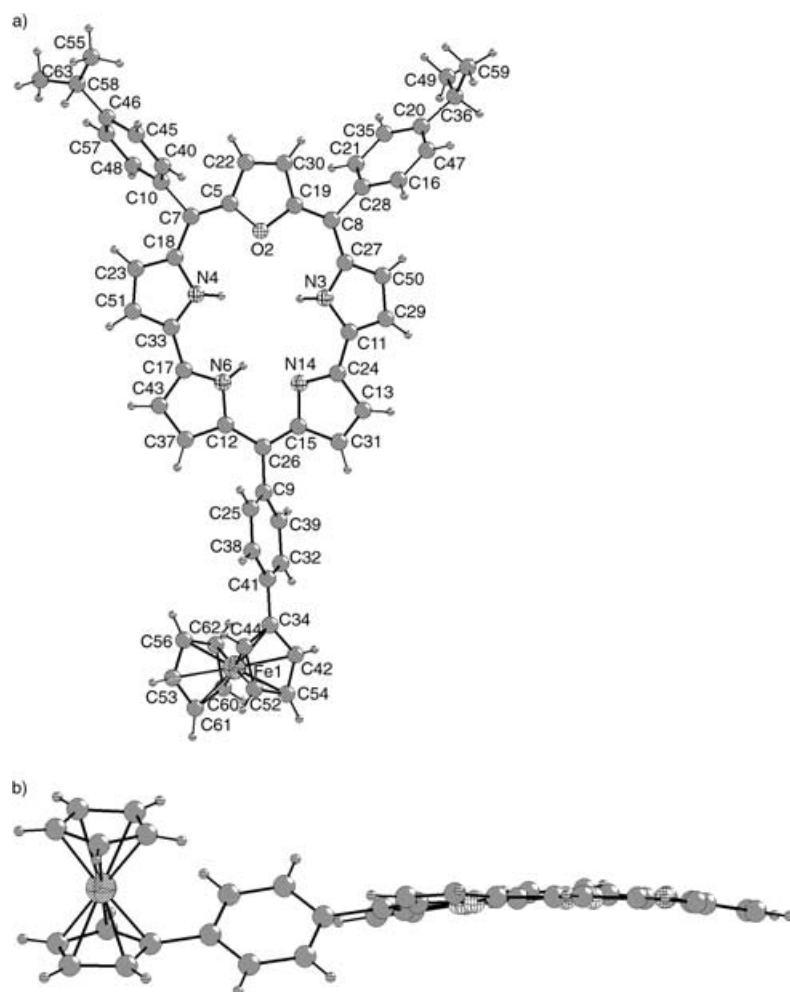


Figure 8. Single crystal X-ray structure of **7d** a) top view; b) side view (*meso*-phenyl rings are omitted for clarity).

*p*-nitroaniline (pNA) as an external reference. It is clearly seen from the Table that the  $\beta$  values for compounds **7a–9c** are roughly 4–5 times larger compared to corresponding, structurally similar tetraphenylporphyrin derivatives,<sup>[21]</sup> which have donor–acceptor group present on *meso* phenyl substituents. This observation clearly suggests that the second order nonlinear optical response can be enhanced by enhancing the availability of mobile electrons in the  $\pi$  skeleton, which in turn can play a key role in enhancing the polarization of molecular system (tetraphenyl porphyrin has 18  $\pi$  electrons where the expanded corrole conjugates have 22  $\pi$  electrons). However it should be mentioned here that the  $\beta$  values observed in the present study are only moderate considering the fact that these macrocycles have large no of  $\pi$  electrons. This is due to the nonplanar orientation of the corrole  $\pi$  system, ferrocene and the spacer. It has been shown that the  $\beta$  values can be increased substantially when the donor–acceptor groups, the  $\pi$  system and the linker are in the same plane, where the effective charge transfer polarization can be increased.<sup>[22]</sup> In the present case the X-ray

crystal structure clearly shows that the ferrocene group, the phenyl linker and the corrole skeleton are not oriented in the same plane thus reducing the  $\beta$  values.

## Conclusion

Syntheses of stable expanded corrole–ferrocene conjugates, with different spacers between ferrocene and corrole, have been achieved in moderately good yields by employing “[3+2]” acid-catalyzed oxidative coupling of appropriate precursors. The molecular first hyperpolarizabilities ( $\beta$ ) measured show larger values for the 22  $\pi$  systems relative to structurally similar 18  $\pi$  porphyrin revealing the fact that nonlinear response can be enhanced by increasing the number of  $\pi$  electrons in conjugation. The covalent linking of ferrocene to macrocycle leads to moderate electronic communication between the ferrocenyl moiety and macrocycle  $\pi$  system as observed from spectroscopy and electrochemical measurements. The single-crystal X-ray structure of **7a** and **7d** confirms the proposed structure. It is anticipated that this research effort in the field of expanded corroles, which has long stood in the shadow of expanded porphyrins, will now receive renewed impetus as a result of easy syntheses of stable *meso*-aryl expanded corroles. Detailed studies in this direction are under way in our laboratory.

## Experimental Section

**Instrumentation:** Electronic spectra were recorded on a Perkin–Elmer Lambda 20 UV/Vis spectrophotometer. Proton NMR spectra were obtained on a 400 MHz Jeol spectrometer in CDCl<sub>3</sub>. FAB-MS spectra were obtained on a Jeol-SX-120/DA6000 spectrometer. The Fluorescence spectra were recorded on a SPEX-Fluorolog F112X spectrofluorimeter. Fluorescence lifetime was measured on a IBH picosecond single photon counting system using a 440 nm IBH NanoLED source and Hamamatsu C4878–02 MCP detector. The fluorescence decay profiles were deconvoluted using IBH data station software V2.1, fitted with mono or biexponential decay.

Table 4. Crystallographic data for 4-ferrocenylphenyl dipyrromethane and expanded corrole–ferrocene conjugates.

	<b>3</b>	<b>7a</b>	<b>7d</b>
solvent for crystallization	CH <sub>2</sub> Cl <sub>2</sub> /hexane	CH <sub>2</sub> Cl <sub>2</sub> /MeOH	CH <sub>2</sub> Cl <sub>2</sub> /MeOH
empirical formula	C <sub>38</sub> H <sub>36</sub> Fe <sub>2</sub> N <sub>4</sub>	C <sub>57</sub> H <sub>48</sub> FeN <sub>4</sub> O	C <sub>57</sub> H <sub>48</sub> FeN <sub>4</sub> O
<i>T</i> [K]	210(2)	210	210
crystal system	orthorhombic	monoclinic	orthorhombic
space group	<i>Pbca</i>	<i>P21/c</i>	<i>Pna21</i>
<i>V</i> [Å <sup>3</sup> ]	3793.4(6)	4421.1(4)	4277(3)
<i>a</i> [Å]	14.5304(14)	15.9431(7)	17.796(5)
<i>b</i> [Å]	10.3167(10)	12.5532(8)	24.892(5)
<i>c</i> [Å]	25.305(2)	22.1151(10)	9.655(5)
<i>α</i> [°]	90.00	90.00	90.00
<i>β</i> [°]	90.00	92.716(4)	90.00
<i>γ</i> [°]	90.00	90.00	90.00
<i>Z</i>	8	4	4
$\rho_{\text{calcd}}$ [Mg m <sup>-3</sup> ]	1.423	1.341	1.337
refl. measured/unique	23104/4603	33413/7562	26660/9929
<i>R</i> (in)	0.0830	0.0517	0.0777
<i>F</i> (000)	1696	1880	1808
limiting indices	−19 ≤ <i>h</i> ≤ 12 −13 ≤ <i>k</i> ≤ 13 −33 ≤ <i>l</i> ≤ 27	−18 ≤ <i>h</i> ≤ 18 −14 ≤ <i>k</i> ≤ 14 −26 ≤ <i>l</i> ≤ 26	−22 ≤ <i>h</i> ≤ 22 −18 ≤ <i>k</i> ≤ 33 −13 ≤ <i>l</i> ≤ 12
GoF ( <i>F</i> <sup>2</sup> )	1.071	0.883	1.121
final <i>R</i> indices [ <i>I</i> > 2σ <i>I</i> ]			
<i>R</i> <sub>1</sub>	0.0632	0.0387	0.0973
<i>wR</i> <sub>2</sub>	0.1185	0.0880	0.187
<i>R</i> indices all data			
<i>R</i> <sub>1</sub>	0.0990	0.0652	0.133
<i>wR</i> <sub>2</sub>	0.1311	0.0940	0.2022

Table 5. Important bond lengths and dihedral angles for **3**, **7a** and **7d**.<sup>[a]</sup>

	<b>3</b>	<b>7a</b>	<b>7d</b>			
bond length [Å]	C5–C10	1.528(4)	C15–C42	1.484(3)	C9–C26	1.481(8)
	C13–C16	1.474(4)	C45–C48	1.478(4)	C34–C41	1.499(8)
			C6–C33	1.507(3)	C8–C28	1.507(7)
			C1–C24	1.507(3)	C7–C10	1.514(8)
dihedral angle [°]	A	14.22(9)	B	56.71(8)	B <sup>1</sup>	45.80(8)
			C	89.98(6)	C <sup>1</sup>	67.66(7)
			D	85.21(5)	D <sup>1</sup>	87.81(9)
			E	22.59(9)	E <sup>1</sup>	22.40(6)
			F	37.15(9)	F <sup>1</sup>	23.48(6)

[a] A is the dihedral angle between phenyl ring and Cp ring of ferrocene; B is the dihedral angle between phenyl ring attached to C15 carbon and expanded corrole plane formed by three *meso* carbons; C is the dihedral angle between mesityl ring attached to C1 carbon and expanded corrole plane formed by three *meso* carbons; D is the dihedral angle between mesityl ring attached to C6 carbon and expanded corrole plane formed by three *meso* carbons; E is the dihedral angle between Cp ring of ferrocene and expanded corrole plane formed by three *meso* carbons; F is the dihedral angle between phenyl ring attached to C15 carbon and Cp ring of ferrocene. Similarly B<sup>1</sup>, C<sup>1</sup>, D<sup>1</sup>, E<sup>1</sup>, and F<sup>1</sup> are the corresponding dihedral angles for compound **7d**.

**X-ray crystallographic studies:** The crystals were immersed in hydrocarbon oil (Paraton N), a single crystal selected, mounted on a glass fiber and placed in the low-temperature N<sub>2</sub> stream.<sup>[15]</sup> Intensity data were collected at 210 K with a Stoe IPDS2 system utilizing MoK<sub>α</sub> radiation (λ = 0.71073 Å). The intensities were corrected for Lorentz and polarization effects. The structure was solved with Direct Methods using the SHELXTL PLUS program system<sup>[16a]</sup> and refined against |*F*<sup>2</sup>| with the program XL-97 by using all data.<sup>[16b]</sup> Hydrogen atoms were placed geometrically and refined by using a riding model, including free rotation about C–C bonds for methyl groups with *U*<sub>iso</sub> constrained at 1.2 for non-

Table 6. Electrochemical data for expanded corrole–ferrocene conjugates along with free ferrocene and dipyrromethanes using 0.1 M TBAPF<sub>6</sub> (tetra-*n*-butylammonium hexafluorophosphate) as the supporting electrolyte in CH<sub>2</sub>Cl<sub>2</sub>, potential range scanned from −1.5 V versus Ag/Ag<sup>+</sup> recorded at 100 mV s<sup>−1</sup> scan speed.

Compound	Expanded ring		Ferrocenyl ring
	<i>E</i> <sub>1/2</sub> <sup>ox</sup> (1) [V]	<i>E</i> <sub>1/2</sub> <sup>ox</sup> (2) [V]	<i>E</i> <sub>1/2</sub> <sup>ox</sup> [V]
<b>Fc</b>	–	–	0.202
<b>3</b>	–	–	0.215
<b>4</b>	–	–	0.293
<b>5</b>	–	–	0.208
<b>1</b>	0.140	0.468	–
<b>2</b>	0.038	0.606	0.296
<b>7a</b>	0.115	0.495	0.258
<b>7b</b>	0.129	0.444	0.260
<b>7c</b>	0.110	0.440	0.248
<b>7d</b>	0.114	0.433	0.250
<b>8a</b>	0.129	0.490	0.329
<b>8b</b>	0.128	0.448	0.319
<b>8c</b>	0.096	0.430	0.324
<b>9a</b>	0.141	0.479	0.245
<b>9b</b>	0.135	0.432	0.240
<b>9c</b>	0.136	0.433	0.245
<b>10</b>	0.209	0.532	0.262
<b>11</b>	0.182	0.538	0.252
<b>12</b>	0.196	0.520	0.248
<b>13</b>	0.181	0.535	0.324
<b>14</b>	0.218	0.527	0.240

methyl groups, and 1.5 for methyl groups times *U*<sub>eq</sub> of the carrier carbon atom. All non hydrogen atoms were refined anisotropically.

CCDC-261725 (**3**), -261726 (**7a**) and -261727 (**7d**) contain the supplementary crystallographic data for this paper. These data can be obtained free of charge from The Cambridge Crystallographic Data Centre via [www.ccdc.cam.ac.uk/data\\_request/cif/](http://www.ccdc.cam.ac.uk/data_request/cif/).

#### Hyper-Rayleigh scattering (HRS)

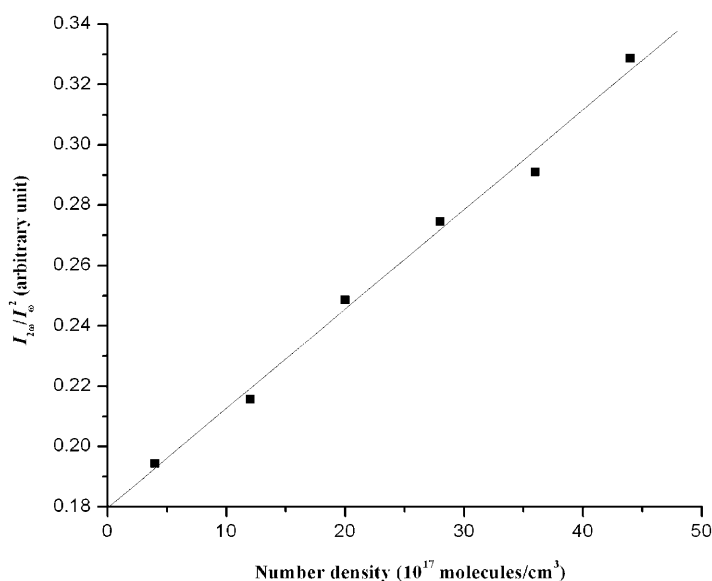
**measurements:** First hyperpolarizability of all the molecules was determined by HRS technique using external reference method. Experiments were carried out in dichloromethane employing a fundamental wavelength (1064 nm) of a Q-switched Nd:YAG laser (Lab 170, Spectra Physics, 10 Hz, 8 ns). All the data were collected at laser powers 17–20 mJ per pulse. The experimental setup used for the HRS measurements was similar to previous description.<sup>[17]</sup> In brief, the exciting beam was focused by a biconvex lens (f.l. 8 cm) to a spot 5 cm away after passing through the cylindrical glass cell containing the sample. A visible photomultiplier tube (PMT) collects

scattered light in the perpendicular direction. A high through-put monochromator (Jobin Yvon, TRIAX 550) was used for wavelength dispersion and no other collection optics was employed. The monochromator was scanned and at each wavelength, the signal output from the PMT was averaged over 256 laser shots. The input power was monitored using a power meter. The intensity of the second harmonic scattered light, *I*<sub>2ω</sub> (taken from peak of Lorentzian fit) for a two component mixture of solvent and solute is given by Equation (3):

$$I_{2\omega} = G\{N_{\text{solvent}} \cdot \beta_{\text{solvent}}^2 + N_{\text{solute}} \cdot \beta_{\text{solute}}^2\} \cdot I_{\omega}^2 \quad (3)$$

Table 7. HRS hyperpolarizabilities ( $\beta$ ) measured at 1064 nm for **7a–11**.

Compound	$\beta$ ( $10^{-30}$ esu)
<b>1</b>	33.3
<b>2</b>	32.8
<b>7a</b>	16.6
<b>7b</b>	27.2
<b>7c</b>	28.5
<b>7d</b>	26.8
<b>8a</b>	20.4
<b>8b</b>	19.9
<b>8c</b>	20.2
<b>9a</b>	30.2
<b>9b</b>	32.9
<b>9c</b>	29.5
<b>10</b>	19.8
<b>11</b>	31.8

Figure 9.  $I_{2\omega}/I_\omega^2$  versus number density of **9b** in  $\text{CH}_2\text{Cl}_2$ . The solid line is best linear fit;  $\beta_{1064\text{ nm}} = 32.9 \times 10^{-30}$  esu, solvent:  $\text{CH}_2\text{Cl}_2$ .

The quadratic coefficient  $I_{2\omega}/I_\omega^2$  varies linearly with number density,  $N_{\text{solute}}$  of the solute, if  $\beta$  and  $N$  for the solvent were fixed. HRS measurements were carried for all compounds in the concentration range varying from  $10^{-5}$ – $10^{-6}$  M. Since low concentrations of solute were used, we assume that the presence of the solute molecules does not change the number density of the solvent molecules,  $N_{\text{solvent}}$  significantly. First the  $\beta$  value of *p*-nitroaniline (pNA) was studied as  $18.7 \times 10^{-30}$  esu in chloroform by external reference method<sup>[18]</sup> using pNA in dioxane as the reference.

**Chemicals:** All NMR solvents were used as received. Solvents like dichloromethane, tetrahydrofuran and *n*-hexane were purified and distilled by standard procedures. Tetra-*n*-butyl ammonium hexafluorophosphate from Fluka was used as the supporting electrolyte for cyclic voltammetric studies. 2,5-Bis(phenyl hydroxy methyl)furan and 16-oxatripyrrane (**6a–d**) were prepared according to the published procedure<sup>[9]</sup> and stored under inert atmosphere at  $-10^\circ\text{C}$ .

#### Syntheses

**4-Ferrocenylbenzaldehyde:** 4-Ferrocenylbenzaldehyde was prepared via suitable modifications of literature procedures.<sup>[19]</sup> Thionyl chloride (1.09 mL, 15 mmol) dropwise over 10 min was added under ice-cooling to a stirred solution of 4-aminobenzoic acid (1.38 g, 10 mmol) in methanol

(15 mL). After stirring the reaction mixture for 3 h, methanol was distilled out and water (25 mL) was added. The separated ester was extracted with ethyl acetate and washed with saturated sodium bicarbonate solution. Drying ( $\text{Na}_2\text{SO}_4$ ) and evaporation of ethyl acetate gave the ester in pure form (1.30 g, 95 %).

The above ester was dissolved in (5 mL  $\text{H}_2\text{SO}_4$  + 10 mL water) in ice bath and to this solution  $\text{NaNO}_2$  (0.7 g, 10 mmol in 5 mL water) was added dropwise at  $0$ – $5^\circ\text{C}$ . The solution was poured immediately to ferrocene (1.67 g, 9 mmol in 100 mL acetic acid) and was stirred over night.  $\text{Et}_2\text{O}$  (200 mL) was added and the workup was done by  $\text{Et}_2\text{O}$  ( $3 \times 200$  mL) and organic layer was washed with sat.  $\text{NaHCO}_3$  and dried over  $\text{MgSO}_4$ . It was then purified by column chromatography over silica gel eluting first with petroleum ether (to remove unreacted ferrocene) and then with ethyl acetate/petroleum ether 5:95; yield: 1.80 g, 60 %.

A solution of methyl 4-ferrocenylbenzoate (1.10 g, 3.4 mmol) in THF (10 mL) was added dropwise to a suspension of  $\text{LiAlH}_4$  (105 mg, 2.7 mmol) in THF (10 mL) the mixture was stirred at room temperature for 2 h under  $\text{N}_2$ . Then it was quenched by ice and aq.  $\text{NaOH}$ .  $\text{Et}_2\text{O}$  (40 mL) was added. The ether layer was washed with water and brine, dried ( $\text{MgSO}_4$ ), and concentrated affording a yellow solid (900 mg, 90 %). A sample of the alcohol (630 mg, 2.16 mmol) was added to a suspension of 2-iodoxybenzoic acid (IBX) in acetone (20 mL). The mixture was stirred under  $\text{N}_2$  at room temperature for 2 h. it was filtered and dried ( $\text{MgSO}_4$ ). The filtrate was concentrated and chromatographed (silica gel, ethyl acetate/hexane 4:96) affording the title compound (540 mg, 88 %). FAB-MS:  $m/z$  (%): 290 (100) [ $M^+$ ];  $^1\text{H NMR}$  (400 MHz,  $\text{CDCl}_3$ ,  $25^\circ\text{C}$ , TMS):  $\delta$  = 9.90 (s, 1H), 7.72 (d,  $J$  = 8 Hz, 2H), 7.52 (d,  $J$  = 8 Hz, 2H), 4.67 ( $\text{A}_2\text{B}_2$ ,  $J$  = 1.6 Hz, 2H), 4.36 ( $\text{A}_2\text{B}_2$ ,  $J$  = 1.6 Hz, 2H), 3.98 (s, 5H); elemental analysis calcd (%) for  $\text{C}_{17}\text{H}_{14}\text{FeO}$ : C 70.37, H 4.86; found: C 70.42, H 4.80.

The respective aldehydes for dipyrromethane **4** and **5** were synthesized by following the general procedure<sup>[19,20]</sup> in the literature.

**5-(4-Ferrocenylphenyl) dipyrromethane (3):** A mixture of pyrrole (3 mL, 43 mmol) and 4-ferrocenylphenyl benzaldehyde (0.5 g, 1.7 mmol) was degassed by bubbling argon for 10 min. Trifluoroacetic acid (0.01 mL, 0.17 mmol) was added, the mixture was stirred at room temperature for 20 min. It was diluted with  $\text{CH}_2\text{Cl}_2$  (50 mL) and then washed with 0.1 M  $\text{NaOH}$ . The organic layer was dried over anhydrous sodium sulfate. The solvent was removed under reduced pressure and the unreacted pyrrole was removed by vacuum distillation at room temperature. The resulting viscous liquid was purified by column chromatography (silica gel (100–200 mesh), ethyl acetate/petroleum ether 5:95), evaporation gave **3** as a pale yellow solid (0.60 g, 75 %); FAB-MS:  $m/z$  (%): 406 (100) [ $M^+$ ];  $^1\text{H NMR}$  (400 MHz,  $\text{CDCl}_3$ ,  $25^\circ\text{C}$ , TMS):  $\delta$  = 7.9 (brs, 2H), 7.35 (d,  $J$  = 8.3 Hz, 2H), 7.06 (d,  $J$  = 8.3 Hz, 2H), 6.65 (m, 2H), 6.1 (m, 2H), 5.87 (d, 2H), 5.39 (s, 1H), 4.53 (t, 2H), 4.23 (t, 2H), 3.97 (s, 5H); elemental analysis calcd (%) for  $\text{C}_{25}\text{H}_{22}\text{N}_2\text{Fe}$ : C 73.87, H 5.45, N 6.89; found: C 73.61, H 5.59, N 6.31.

The above procedure was followed using respective aldehydes to get other dipyrromethanes.

**Compound 4:** FAB-MS:  $m/z$  (%): 430 (100) [ $M^+$ ];  $^1\text{H NMR}$  (400 MHz,  $\text{CDCl}_3$ ,  $25^\circ\text{C}$ , TMS):  $\delta$  = 7.92 (brs, 2H), 7.42 (d,  $J$  = 8.1 Hz, 2H), 7.16 (d,  $J$  = 8.1 Hz, 2H), 6.70 (d, 2H), 6.16 (m, 2H), 5.91 (d, 2H), 5.46 (s, 1H), 4.49 (t, 2H), 4.23 (m, 7H); elemental analysis calcd (%) for  $\text{C}_{27}\text{H}_{22}\text{N}_2\text{Fe}$ : C 75.32, H 5.15, N 6.51; found: C 75.21, H 5.59, N 6.42.

**Compound 5:** FAB-MS:  $m/z$  (%): 506 (100) [ $M^+$ ];  $^1\text{H NMR}$  (400 MHz,  $\text{CDCl}_3$ ,  $25^\circ\text{C}$ , TMS):  $\delta$  = 7.95 (brs, 2H), 7.47 (m, 6H), 7.20 (d, 2H), 6.72 (d, 2H), 6.17 (m, 2H), 5.90 (d, 2H), 5.49 (s, 1H), 4.66 (d,  $J$  = 1.6 Hz, 2H), 4.35 (d,  $J$  = 1.6 Hz, 2H), 4.03 (s, 5H); elemental analysis calcd (%) for  $\text{C}_{33}\text{H}_{26}\text{N}_2\text{Fe}$ : C 78.23, H 5.17, N 5.53; found: C 78.01, H 5.39, N 5.31.

**5,10-Mesityl-19-(4-ferrocenylphenyl)-25-oxa smaragdyrin (7a):** Oxatripyrrane **6a** (0.406 g, 0.869 mmol) and 5-(4-ferrocenylphenyl)dipyrromethane **3** (0.350 g, 0.869 mmol) were dissolved in dry dichloromethane (250 mL) and stirred under nitrogen atmosphere for 5 min. TFA (0.006 mL, 0.089 mmol) was added and the stirring was continued for further 90 min. Chloranil (0.640 g, 2.6 mmol) was added and the reaction mixture was exposed to air and heated under reflux for a further 90 min. The solvent

was evaporated in vacuum. The residue was purified by chromatography on a basic alumina column, second green band which eluted with dichloromethane gave **7a** (0.18 g, 25%), which decomposed above 320°C. FAB-MS: *m/z* (%): 862 (100) [(*M*+2)<sup>+</sup>]; <sup>1</sup>H NMR (400 MHz, CDCl<sub>3</sub>, 25°C, TMS): δ = 9.34 (d, *J* = 4.2 Hz, 2H), 9.26 (d, *J* = 4.2 Hz, 2H), 8.92 (d, *J* = 4.2 Hz, 2H), 8.47 (s, 2H), 8.25 (d, *J* = 4.2 Hz, 2H), 8.24 (d, *J* = 7.8 Hz, 2H), 7.86 (d, *J* = 7.8 Hz, 2H), 7.25 (s, 1H), 4.87 (s, 2H), 4.42 (s, 2H), 4.42 (s, 2H), 4.2 (s, 5H), 2.57 (s, 6H), 1.86 (s, 12H); UV/Vis (CH<sub>2</sub>Cl<sub>2</sub>): λ<sub>max</sub> (ε × 10<sup>-4</sup> M<sup>-1</sup> cm<sup>-1</sup>): 447 (17.34), 555 (1.29), 594 (1.05), 636 (0.9), 700 nm (1.21); (CH<sub>2</sub>Cl<sub>2</sub>/TFA): λ<sub>max</sub> (ε × 10<sup>-4</sup> M<sup>-1</sup> cm<sup>-1</sup>): 452 (11.7), 485 (sh, 5.7), 610 (0.6), 662 (0.8), 730 nm (2.4); elemental analysis calcd (%) for C<sub>57</sub>H<sub>48</sub>N<sub>4</sub>OFe: C 79.51, H 5.61, N 6.51; found: C 79.01, H 5.59, N 6.31. The above procedure was followed using respective oxatripyrranes **7b–9c** to get other expanded corrole–ferrocene conjugates.

**Compound 7b:** FAB-MS: *m/z* (%): 805 (100) [*M*+H<sup>+</sup>]; <sup>1</sup>H NMR (400 MHz, CDCl<sub>3</sub>, 25°C, TMS): δ = 9.37 (d, 2H), 9.29 (d, 2H), 8.94 (d, 2H), 8.66 (s, 2H), 8.34 (d, 2H), 8.24 (d, 2H), 8.00 (d, 4H), 7.88 (d, 2H), 7.52 (d, 4H), 4.86 (s, 2H), 4.41 (t, 2H), 4.20 (s, 5H), 2.65 (s, 6H); UV/Vis (CH<sub>2</sub>Cl<sub>2</sub>): λ<sub>max</sub> (ε × 10<sup>-4</sup> M<sup>-1</sup> cm<sup>-1</sup>): 446 (18.9), 555 (1.4), 594 (1.0), 637 (0.8), 700 nm (1.3); (CH<sub>2</sub>Cl<sub>2</sub>/TFA): λ<sub>max</sub> (ε × 10<sup>-4</sup> M<sup>-1</sup> cm<sup>-1</sup>): 452 (15.6), 484 (sh, 6.2), 610 (1.2), 668 (1.5), 736 nm (3.2); elemental analysis calcd (%) for C<sub>53</sub>H<sub>40</sub>N<sub>4</sub>OFe: C 79.07, H 5.01, N 6.96; found: C 78.81, H 4.89, N 7.11.

**Compound 7c:** FAB-MS: *m/z* (%): 890 (100) [(*M*+2)<sup>+</sup>]; <sup>1</sup>H NMR (400 MHz, CDCl<sub>3</sub>, 25°C, TMS): δ = 9.46 (d, *J* = 4 Hz, 2H), 9.38 (d, *J* = 3.6 Hz, 2H), 9.03 (d, *J* = 3.6 Hz, 2H), 8.75 (s, 2H), 8.47 (d, *J* = 4 Hz, 2H), 8.32 (d, *J* = 7.6 Hz, 2H), 8.13 (d, *J* = 8 Hz, 4H), 7.96 (d, *J* = 7.6 Hz, 2H), 7.81 (d, *J* = 8 Hz, 4H), 4.94 (s, 2H), 4.50 (d, 2H), 4.29 (s, 5H), 1.65 (d, 18H); UV/Vis (CH<sub>2</sub>Cl<sub>2</sub>): λ<sub>max</sub> (ε × 10<sup>-4</sup> M<sup>-1</sup> cm<sup>-1</sup>): 446 (18.2), 554 (1.5), 594 (1), 637 (0.9), 700 nm (1.3); (CH<sub>2</sub>Cl<sub>2</sub>/TFA): λ<sub>max</sub> (ε × 10<sup>-4</sup> M<sup>-1</sup> cm<sup>-1</sup>): 452 (15.3), 486 (sh, 5.3), 607 (0.5), 664 (0.4), 733 nm (2.5); elemental analysis calcd (%) for C<sub>59</sub>H<sub>52</sub>N<sub>4</sub>OFe: C 79.67, H 5.89, N 6.33; found: C 79.61, H 5.69, N 6.39.

**Compound 7d:** FAB-MS: *m/z* (%): 861 (100) [*M*+H<sup>+</sup>]; <sup>1</sup>H NMR (400 MHz, CDCl<sub>3</sub>, 25°C, TMS): δ = 9.37 (d, 2H), 9.29 (d, 2H), 8.94 (d, 2H), 8.67 (s, 2H), 8.36 (d, 2H), 8.24 (d, *J* = 7.6 Hz, 2H), 8.03 (d, *J* = 7.3 Hz, 4H), 7.87 (d, *J* = 7.6 Hz, 2H), 7.57 (d, *J* = 7.3 Hz, 4H), 4.86 (t, 2H), 4.42 (t, 2H), 4.19 (s, 5H), 3.21 (t, 2H), 1.49 (d, 12H); UV/Vis (CH<sub>2</sub>Cl<sub>2</sub>): λ<sub>max</sub> (ε × 10<sup>-4</sup> M<sup>-1</sup> cm<sup>-1</sup>): 446 (18.2), 554 (1.5), 594 (1.0), 637 (0.9), 700 nm (1.4); (CH<sub>2</sub>Cl<sub>2</sub>/TFA): λ<sub>max</sub> (ε × 10<sup>-4</sup> M<sup>-1</sup> cm<sup>-1</sup>): 452 (14.3), 485 (sh), 608 (5.9), 665 (1.2), 734 nm (2.6); elemental analysis calcd (%) for C<sub>57</sub>H<sub>48</sub>N<sub>4</sub>OFe: C 79.51, H 5.61, N 6.51; found: C 78.91, H 5.59, N 6.31.

**Compound 8a:** FAB-MS: *m/z* (%): 886 (100) [(*M*+2)<sup>+</sup>]; <sup>1</sup>H NMR (400 MHz, CDCl<sub>3</sub>, 25°C, TMS): δ = 9.46 (d, *J* = 4.4 Hz, 2H), 9.37 (d, *J* = 4 Hz, 2H), 8.95 (d, *J* = 4 Hz, 2H), 8.59 (s, 2H), 8.37 (d, *J* = 4.4 Hz, 2H), 8.35 (d, *J* = 8.4 Hz, 2H), 7.97 (d, *J* = 8.4 Hz, 2H), 7.33 (s, 4H), 4.67 (t, 2H), 4.38 (d, 7H), 2.65 (s, 6H), 1.92 (s, 12H); UV/Vis (CH<sub>2</sub>Cl<sub>2</sub>): λ<sub>max</sub> (ε × 10<sup>-4</sup> M<sup>-1</sup> cm<sup>-1</sup>): 450 (22.5), 557 (1.9), 597 (1.6), 639 (1.4), 703 nm (1.9); (CH<sub>2</sub>Cl<sub>2</sub>/TFA): λ<sub>max</sub> (ε × 10<sup>-4</sup> M<sup>-1</sup> cm<sup>-1</sup>): 454 (18.6), 485 (sh, 6.8), 610 (1.1), 662 (1.3), 730 nm (3.2); elemental analysis calcd (%) for C<sub>59</sub>H<sub>48</sub>N<sub>4</sub>OFe: C 80.06, H 5.47, N 6.33; found: C 80.01, H 5.59, N 6.41.

**Compound 8b:** FAB-MS: *m/z* (%): 852 (100) [(*M*+2)<sup>+</sup>]; <sup>1</sup>H NMR (400 MHz, CDCl<sub>3</sub>, 25°C, TMS): δ = 9.51 (d, *J* = 4.2 Hz, 2H), 9.41 (d, *J* = 4.1 Hz, 2H), 8.99 (d, *J* = 4.1 Hz, 2H), 8.78 (s, 2H), 8.48 (d, *J* = 4.2 Hz, 2H), 8.37 (d, *J* = 8.0 Hz, 2H), 8.09 (d, *J* = 7.8 Hz, 4H), 7.97 (d, *J* = 8.0 Hz, 2H), 7.62 (d, *J* = 7.8 Hz, 4H), 4.67 (s, 2H), 4.35 (m, 7H), 2.73 (s, 6H); UV/Vis (CH<sub>2</sub>Cl<sub>2</sub>): λ<sub>max</sub> (ε × 10<sup>-4</sup> M<sup>-1</sup> cm<sup>-1</sup>): 448 (21.6), 555 (1.5), 595 (1.2), 640 (0.9), 703 nm (1.5); (CH<sub>2</sub>Cl<sub>2</sub>/TFA): λ<sub>max</sub> (ε × 10<sup>-4</sup> M<sup>-1</sup> cm<sup>-1</sup>): 453 (19.5), 485 (sh, 6.8), 609 (1.3), 664 (1.5), 733 nm (3.4); elemental analysis calcd (%) for C<sub>57</sub>H<sub>40</sub>N<sub>4</sub>OFe: C 80.25, H 4.73, N 6.57; found: C 80.01, H 4.59, N 6.41.

**Compound 8c:** FAB-MS: *m/z* (%): 914 (100) [(*M*+2)<sup>+</sup>]; <sup>1</sup>H NMR (400 MHz, CDCl<sub>3</sub>, 25°C, TMS): δ = 9.51 (d, 2H), 9.42 (d, 2H), 9.00 (d, 2H), 8.78 (s, 2H), 8.50 (d, 2H), 8.36 (d, 2H), 8.13 (d, 2H), 7.98 (d, 2H), 7.82 (d, 4H), 4.62 (s, 2H), 4.37 (d, 7H), 1.67 (s, 18H); UV/Vis (CH<sub>2</sub>Cl<sub>2</sub>): λ<sub>max</sub> (ε × 10<sup>-4</sup> M<sup>-1</sup> cm<sup>-1</sup>): 449 (19.5), 556 (1.6), 595 (1.3), 639 (1), 703 nm (1.5); (CH<sub>2</sub>Cl<sub>2</sub>/TFA): λ<sub>max</sub> (ε × 10<sup>-4</sup> M<sup>-1</sup> cm<sup>-1</sup>): 454 (14.5), 485 (sh, 4.6), 612

(1.1), 665 (1.2), 733 nm (3.2); elemental analysis calcd (%) for C<sub>61</sub>H<sub>52</sub>N<sub>4</sub>OFe: C 80.23, H 5.74, N 6.13; found: C 80.01, H 5.80, N 6.21.

**Compound 9a:** FAB-MS: *m/z* (%): 962 (50) [(*M*+2)<sup>+</sup>]; <sup>1</sup>H NMR (400 MHz, CDCl<sub>3</sub>, 25°C, TMS): δ = 9.46 (d, *J* = 4.2 Hz, 2H), 9.37 (d, *J* = 4.3 Hz, 2H), 8.97 (d, *J* = 4.3 Hz, 2H), 8.59 (s, 2H), 8.39 (d, *J* = 4.2 Hz, 2H), 8.37 (d, 2H), 8.02 (d, 2H), 7.62 (d, *J* = 8.1 Hz, 2H), 7.50 (d, *J* = 8.1 Hz, 2H), 7.34 (m, 4H), 4.73 (d, 2H), 4.39 (s, 2H), 4.09 (s, 5H), 2.65 (s, 6H), 1.92 (s, 12H); UV/Vis (CH<sub>2</sub>Cl<sub>2</sub>): λ<sub>max</sub> (ε × 10<sup>-4</sup> M<sup>-1</sup> cm<sup>-1</sup>): 451 (23.2), 557 (1.6), 596 (1.3), 640 (1.1), 704 nm (1.6); (CH<sub>2</sub>Cl<sub>2</sub>/TFA): λ<sub>max</sub> (ε × 10<sup>-4</sup> M<sup>-1</sup> cm<sup>-1</sup>): 455 (19.5), 485 (sh, 6.7), 612 (1.5), 662 (1.7), 730 (4.6); elemental analysis calcd (%) for C<sub>65</sub>H<sub>52</sub>N<sub>4</sub>OFe: C 81.22, H 5.45, N 5.83; found: C 81.28, H 5.59, N 5.90.

**Compound 9b:** FAB-MS: *m/z* (%): 906 (100) [(*M*+2)<sup>+</sup>]; <sup>1</sup>H NMR (400 MHz, CDCl<sub>3</sub>, 25°C, TMS): δ = 9.51 (d, 2H), 9.42 (d, 2H), 8.99 (d, 2H), 8.78 (s, 2H), 8.49 (d, 2H), 8.40 (d, 2H), 8.09 (m, 8H), 7.61 (m, 4H), 7.55 (d, 2H), 4.73 (s, 2H), 4.39 (s, 2H), 4.10 (s, 5H), 2.73 (s, 6H); UV/Vis (CH<sub>2</sub>Cl<sub>2</sub>): λ<sub>max</sub> (ε × 10<sup>-4</sup> M<sup>-1</sup> cm<sup>-1</sup>): 450 (24.8), 556 (1.7), 595 (1.4), 640 (1), 704 nm (1.7); (CH<sub>2</sub>Cl<sub>2</sub>/TFA): λ<sub>max</sub> (ε × 10<sup>-4</sup> M<sup>-1</sup> cm<sup>-1</sup>): 455 (21.3), 485 (sh, 7.2), 610 (1.6), 664 (1.8), 733 nm (4.3); elemental analysis calcd (%) for C<sub>61</sub>H<sub>44</sub>N<sub>4</sub>OFe: C 80.94, H 4.91, N 6.19; found: C 80.81, H 4.99, N 6.31.

**Compound 9c:** FAB-MS: *m/z* (%): 990 (100) [(*M*+2)<sup>+</sup>]; <sup>1</sup>H NMR (400 MHz, CDCl<sub>3</sub>, 25°C, TMS): δ = 9.52 (d, 2H), 9.43 (d, 2H), 9.00 (d, 2H), 8.80 (s, 2H), 8.51 (d, 2H), 8.40 (d, *J* = 7.8 Hz, 2H), 8.14 (d, *J* = 7.8 Hz, 4H), 8.04 (d, *J* = 8.3 Hz, 2H), 7.81 (d, *J* = 7.8 Hz, 4H), 7.62 (d, *J* = 7.8 Hz, 2H), 7.55 (d, *J* = 8.3 Hz, 2H), 4.73 (d, 2H), 4.34 (d, 2H), 4.10 (s, 5H), 1.63 (s, 18H); UV/Vis (CH<sub>2</sub>Cl<sub>2</sub>): λ<sub>max</sub> (ε × 10<sup>-4</sup> M<sup>-1</sup> cm<sup>-1</sup>): 450 (24.6), 556 (1.3), 594 (1.1), 640 (0.9), 704 nm (1.6); (CH<sub>2</sub>Cl<sub>2</sub>/TFA): λ<sub>max</sub> (ε × 10<sup>-4</sup> M<sup>-1</sup> cm<sup>-1</sup>): 455 (20.7), 486 (sh, 5.2), 610 (1.3), 664 (1.4), 734 nm (3.9); elemental analysis calcd (%) for C<sub>67</sub>H<sub>56</sub>N<sub>4</sub>OFe: C 81.34, H 5.71, N 5.66; found: C 81.11, H 5.59, N 5.53.

**(5,10-(*p*-Methyl-diphenyl)-19-(4-ferrocenylphenyl)-25-oxasamaragdyrina-to) dicarbonyl rhodium-(I) (10):** Compound **7b** (0.030 g, 0.037 mmol) was dissolved in alcohol-free dichloromethane (40 mL). Anhydrous sodium acetate (0.030 g, 0.37 mmol) was added to the solution followed by di-μ-chlorobis[dicarbonylrhodium(II)] (0.020 g, 0.05 mmol), and the mixture was stirred under reflux for 2 h. The solvent was evaporated and was chromatographed by using a silica gel column with dichloromethane solution. Removal of the solvent gave a purple solid (0.032 g, 95%), which was recrystallized from a dichloromethane/*n*-hexane mixture. FAB-MS: *m/z* (%): 961 (70) [*M*+H<sup>+</sup>]; <sup>1</sup>H NMR (400 MHz, CDCl<sub>3</sub>, 25°C, TMS): δ = 9.44 (dd, 2H), 9.12 (d, *J* = 4.4 Hz, 2H), 8.77 (d, *J* = 4.4 Hz, 2H), 8.76 (s, 2H), 8.45 (dd, 2H), 8.13 (m, 4H), 7.97 (d, 2H), 7.84 (d, 2H), 7.55 (m, 4H), 4.47 (s, 2H), 4.42 (s, 2H), 4.20 (s, 5H), 2.66 (s, 6H), -1.77 (s, 2H); IR (KBr):  $\tilde{\nu}$  = 2007, 2072 cm<sup>-1</sup>; UV/Vis (CH<sub>2</sub>Cl<sub>2</sub>): λ<sub>max</sub> (ε × 10<sup>-4</sup> M<sup>-1</sup> cm<sup>-1</sup>): 459 (14.6), 573 (1.5), 616 (1.3), 637 (1.5), 700 nm (2.4); elemental analysis calcd (%) for C<sub>55</sub>H<sub>38</sub>N<sub>4</sub>O<sub>3</sub>FeRh: C 68.66, H 3.98, N 5.83; found: C 68.51, H 5.89, N 5.91.

The above procedure was followed using expanded corrole–ferrocene conjugates **7c**, **7d**, **8c** and **9c** to get other rhodium-expanded corrole complexes.

**Compound 11:** FAB-MS: *m/z* (%): 1047 (50) [(*M*+2)<sup>+</sup>]; <sup>1</sup>H NMR (400 MHz, CDCl<sub>3</sub>, 25°C, TMS): δ = 9.50 (dd, 2H), 9.19 (d, 2H), 8.84 (s, 2H), 8.83 (d, 2H), 8.54 (dd, 2H), 8.24 (m, 4H), 8.09 (d, 2H), 7.91 (d, 2H), 7.82 (m, 4H), 4.94 (d, 2H), 4.50 (s, 2H), 4.27 (s, 5H), 1.64 (s, 18H), -1.69 (s, 2H); IR (KBr):  $\tilde{\nu}$  = 2006, 2071 cm<sup>-1</sup>; UV/Vis (CH<sub>2</sub>Cl<sub>2</sub>): λ<sub>max</sub> (ε × 10<sup>-4</sup> M<sup>-1</sup> cm<sup>-1</sup>): 459 (14.6), 479 (0.9), 573 (1.7), 616 (1.5), 638 nm (1.4); elemental analysis calcd (%) for C<sub>61</sub>H<sub>50</sub>N<sub>4</sub>O<sub>3</sub>FeRh: C 70.03, H 4.82, N 5.35; found: C 70.11, H 4.73, N 5.39.

**Compound 12:** FAB-MS: *m/z* (%): 1018 (65) [*M*+H<sup>+</sup>]; <sup>1</sup>H NMR (400 MHz, CDCl<sub>3</sub>, 25°C, TMS): δ = 9.50 (dd, 2H), 9.19 (d, 2H), 8.84 (d, 2H), 8.82 (s, 2H), 8.54 (dd, 2H), 8.23 (m, 4H), 8.07 (d, 2H), 7.92 (d, 2H), 7.66 (m, 4H), 4.94 (s, 2H), 4.49 (s, 2H), 4.28 (s, 5H), 3.24 (m, 2H), 1.56 (d, 12H), -1.70 (s, 2H); IR (KBr):  $\tilde{\nu}$  = 2007, 2072 cm<sup>-1</sup>; UV/Vis (CH<sub>2</sub>Cl<sub>2</sub>): λ<sub>max</sub> (ε × 10<sup>-4</sup> M<sup>-1</sup> cm<sup>-1</sup>): 459 (12.9), 479 (0.7), 572 (1.5), 616 (1.2), 638 nm (1.2); elemental analysis calcd (%) for C<sub>59</sub>H<sub>46</sub>N<sub>4</sub>O<sub>3</sub>FeRh: C 69.60, H 4.55, N 5.50; found: C 69.51, H 4.50, N 5.53.

**Compound 13:** FAB-MS:  $m/z$  (%): 1071 (40) [( $M+2$ )<sup>+</sup>]; <sup>1</sup>H NMR (400 MHz, CDCl<sub>3</sub>, 25 °C, TMS):  $\delta$  = 9.54 (dd, 2H), 9.22 (d,  $J$  = 4.2 Hz, 2H), 8.88 (s, 2H), 8.78 (d,  $J$  = 4.2 Hz, 2H), 8.57 (dd, 2H), 8.25 (m, 4H), 8.09 (d, 2H), 7.93 (d, 2H), 7.80 (m, 4H), 4.66 (s, 2H), 4.34 (s, 7H), 1.62 (s, 18H), -1.77 (s, 2H); IR (KBr):  $\tilde{\nu}$  = 2008, 2072 cm<sup>-1</sup>; UV/Vis (CH<sub>2</sub>Cl<sub>2</sub>):  $\lambda_{\text{max}}$  ( $\epsilon \times 10^{-4} \text{ M}^{-1} \text{ cm}^{-1}$ ): 460 (18.6), 479 (1.5), 575 (1.1), 617 (0.8), 639 nm (1.2); elemental analysis calcd (%) for C<sub>63</sub>H<sub>50</sub>N<sub>4</sub>O<sub>3</sub>FeRh: C 70.70, H 4.71, N 5.23; found: C 70.61, H 4.60, N 5.31.

**Compound 14:** FAB-MS:  $m/z$  (%): 1147 (35) [( $M+2$ )<sup>+</sup>]; <sup>1</sup>H NMR (400 MHz, CDCl<sub>3</sub>, 25 °C, TMS):  $\delta$  = 9.55 (dd, 2H), 9.23 (d,  $J$  = 4.2 Hz, 2H), 8.89 (s, 2H), 8.80 (d,  $J$  = 4.2 Hz, 2H), 8.59 (dd, 2H), 8.26 (d, 2H), 8.11 (d, 2H), 8.07 (d, 2H), 7.82 (m, 2H), 7.63 (d, 2H), 7.53 (m, 4H), 4.73 (s, 2H), 4.40 (s, 2H), 4.10 (s, 5H), 1.64 (s, 18H), -1.89 (s, 2H); IR (KBr):  $\tilde{\nu}$  = 2008, 2072 cm<sup>-1</sup>; UV/Vis (CH<sub>2</sub>Cl<sub>2</sub>):  $\lambda_{\text{max}}$  ( $\epsilon \times 10^{-4} \text{ M}^{-1} \text{ cm}^{-1}$ ): 461 (19.9), 480 (1.6), 576 (1.4), 619 (0.9), 639 nm (1.4); elemental analysis calcd (%) for C<sub>69</sub>H<sub>54</sub>N<sub>4</sub>O<sub>3</sub>FeRh: C 72.27, H 4.75, N 4.89; found: C 72.11, H 4.64, N 4.71.

### Acknowledgements

This work was supported by grants from the Department of Science and Technology (DST) and Council of Scientific and Industrial Research (CSIR), Government of India, New Delhi. We thank Prof. P. K. Das, IISc, Bangalore for NLO measurements. R.K. thanks the CSIR for Shyama Prasad Mukherjee fellowship. R.M. and V.P.R. thank the CSIR for their fellowships.

- [1] J. L. Sessler, A. Gebauer, E. Vogel in *The Porphyrin Handbook*; Vol. 2 (Eds.: K. M. Kadish, K. M. Smith, R. Guilard), Academic Press, San Diego, **2000**, pp. 1–49, Chapter 8.
- [2] T. K. Chandrashekar, S. Venkatraman, *Acc. Chem. Res.* **2003**, *36*, 676–691.
- [3] J. L. Sessler, D. Seidel, *Angew. Chem.* **2003**, *115*, 5292–5333; *Angew. Chem. Int. Ed.* **2003**, *42*, 5134–5175.
- [4] a) R. Paolesse in *The Porphyrin Handbook*; Vol. 2 (Eds.: K. M. Kadish, K. M. Smith, R. Guilard), Academic Press, San Diego, **2000**, Chapter 11, pp. 201–220; b) S. J. Narayanan, B. Sridevi, T. K. Chandrashekar, *Org. Lett.* **1999**, *1*, 587–590; c) B. Sridevi, S. J. Narayanan, T. K. Chandrashekar, U. Englisch, K. Senge, *Chem. Eur. J.* **2000**, *6*, 2554–2563.
- [5] S. Ery-Forgues, B. Nelvaux-Nicot, *J. Photochem. Photobiol. A* **2000**, *132*, 137–159.
- [6] a) L. M. Tolbert, X. Zhao, Y. Ding, L. A. Bottomley, *J. Am. Chem. Soc.* **1995**, *117*, 12891–12892; b) R. M. Metzger, C. A. Panetta, *New J. Chem.* **1991**, *15*, 209–221.
- [7] a) S. Venkatraman, R. Kumar, J. Sankar, T. K. Chandrashekar, K. Sendhil, C. Vijayan, A. Kelling, M. O. Senge, *Chem. Eur. J.* **2004**, *10*, 1423–1432; b) A. K. Burrell, W. M. Campbell, D. L. Officer, S. M. Scott, K. C. Gordon, M. R. McDonald, *J. Chem. Soc. Dalton Trans.* **1999**, 3349–3354; c) E. S. Schmidt, T. S. Calderwood, T. C. Bruce, *Inorg. Chem.* **1986**, *25*, 3718–3720; d) P. D. Beer, M. G. B. Drew, D. Heseck, R. Jagessar, *J. Chem. Soc. Chem. Commun.* **1995**, 1187–1189; e) S. Venkatraman, V. Prabhuraja, R. Misra, R. Kumar, T. K. Chandrashekar, W. Teng, K. R. Senge, *Ind. J. Chem.* **2003**, *42A*, 2191–2197.
- [8] a) J. H. Chou, M. E. Kosal, H. S. Nalwa, N. A. Rakow, K. S. Suslick, *Porphyrin Handbook*; Vol. VI (Eds.: K. M. Kadish, K. M. Smith, R. Guilard), Academic Press, San Diego, **1999**, pp. 43–131, Chapter 41; b) A. Tsuda, A. Osuka, *Science* **2001**, *293*, 79–82.
- [9] B. Sridevi, S. J. Narayan, A. Srinivasan, M. V. Reddy, T. K. Chandrashekar, *J. Porphyrins Phthalocyanines* **1998**, *2*, 69–78.
- [10] A. Srinivasan, B. Sridevi, M. V. Reddy, S. Jeyaprakash Narayan, T. K. Chandrashekar, *Tetrahedron Lett.* **1997**, *38*, 4149–4152.
- [11] S. J. Narayan, B. Sridevi, T. K. Chandrashekar, A. Vij, R. Roy, *J. Am. Chem. Soc.* **1999**, *121*, 9053–9068.
- [12] a) S. J. Narayanan, B. Sridevi, T. K. Chandrashekar, U. Englisch, K. R. Senge, *Inorg. Chem.* **2001**, *40*, 1637–1645; b) B. Sridevi, S. J. Narayanan, R. Rao, T. K. Chandrashekar, U. Englisch, K. R. Senge, *Inorg. Chem.* **2000**, *39*, 3669–3677.
- [13] M. Gouterman, *The Porphyrins*, Vol. III (Ed.: D. Dolphin), Academic Press, New York, **1978**, pp. 1–165.
- [14] a) D. R. James, Y.-S. Liu, P. De Mayo, W. R. Ware, *Chem. Phys. Lett.* **1985**, *120*, 460–465; b) Y. H. Kim, H. S. Chao, D. Kim, S. K. Kim, N. Yoshida, A. Osuka, *Synth. Met.* **2001**, *117*, 183–187; c) H. N. Fonda, J. V. Gilbert, R. A. Comier, J. R. Sprague, K. Kamioka, J. S. Connolly, *J. Phys. Chem.* **1993**, *97*, 7024–7033.
- [15] H. Hope, *Prog. Inorg. Chem.* **1994**, *41*, 1–19.
- [16] a) G. M. Sheldrick, SHELXS-93f, Universität Göttingen, **1993**; b) G. M. Sheldrick, SHELXL-97, Universität Göttingen, **1997**.
- [17] T. Kodaira, A. Watanabe, O. Ito, M. Matsuda, K. Clays, A. Persoons, *J. Chem. Soc. Faraday Trans.* **1997**, *93*, 3039–3044.
- [18] P. C. Ray, P. K. Das, *J. Phys. Chem.* **1995**, *99*, 14414–14417.
- [19] D. T. Gryko, F. Zhao, A. A. Yasserli, K. M. Roth, D. F. Bocian, W. G. Kuhr, J. L. Lindsey, *J. Org. Chem.* **2000**, *65*, 7356–7362.
- [20] S. Takahashi, Y. Kuroyama, K. Sonogashira, N. Hagihara, *Synthesis* **1980**, 627–628.
- [21] A. Sen, P. C. Ray, P. K. Das, V. Krsihnan, *J. Phys. Chem.* **1996**, *100*, 19601–19613.
- [22] S. M. Lecours, H. W. Guan, S. G. DiMango, C. H. Wang, M. J. Thermen, *J. Am. Chem. Soc.* **1996**, *118*, 1497–1503.

Received: January 29, 2005  
Published online: July 20, 2005